Low-energy Gamow-Teller transitions in deformed $N = Z$ odd-odd nuclei

Hiroyuki Morita and Yoshiko Kanada-En'yo

Department of Physics, Kyoto University, Kyoto 606-8502, Japan

We investigated the Gamow-Teller (GT) transitions from ^{22}Ne to ^{22}Na by applying the isospin projected antisymmetrized molecular dynamics combined with the generator coordinate method. We found that the GT strength from $^A Z(J^\pi T) = {}^{22}\text{Ne}(0_1^+ 1)$ is fragmented into two final states $^{22}\text{Na}(1_{1,2}^+ 0)$, which belong to $K = 0$ and $K = 1$ bands constructed by a prolately deformed ^{20}Ne core with an $S = 1$ proton-neutron (pn) pair. Coupling of the intrinsic spin of the pn pair with the core deformation plays an important role in the GT fragmentation. The symmetry breaking in the intrinsic-spin rotation leads to the SU(4) symmetry breaking of the NN pair and causes the GT fragmentation. We compare the features of the GT transitions with those for $^{10}\text{Be} \rightarrow {}^{10}\text{B}$ and discuss the link between the SU(4) symmetry and the GT fragmentation in deformed systems.

I. INTRODUCTION

Proton-neutron (pn) correlation plays important roles in structure properties of $N = Z$ odd-odd nuclei (see Ref. [1] and references therein). The Gamow-Teller (GT) transition is a good probe for isoscalar pn correlations in $N = Z$ odd-odd nuclei. Effects of the pn pairing on $B(\text{GT})$ have been studied for $N = Z$ odd-odd nuclei in light- and medium-mass regions with a three-body model of two nucleons around spherical cores [2]. One of the interesting features of the GT transitions obtained in $N = Z$ odd-odd nuclei with the LS-closed core (^{4}He, ^{16}O, ^{40}Ca) is the remarkably strong GT transition from $J^\pi T = 0_1^+ 1$ to $1_1^+ 0$, almost exhausting the sum-rule value. The concentration of the GT transition, called the low-energy super-GT transition (LESGT), is described by the transition between dineutron (nn) and deuteron-like pn pairs around the LS-closed core [3].

The GT strength functions of $0_1^+ 1 \rightarrow 1_n^+ 0$ transitions in the pf-shell region have been systematically measured using $(^3\text{He}, t)$ charge-exchange reactions [4]. The measurements have shown that $B(\text{GT}; 0_1^+ 1 \rightarrow 1_1^+ 0)$ is concentrated on the single $1^+ 0$ state in the ^{42}Ca target, but, as the mass number increases from $A = 42$ to $A = 54$, the fragmentation of the GT strengths into many $1^+ 0$ states occurs. The GT fragmentation in this mass region can be understood by configuration mixing of the particle-hole excited states in the spherical pf shell.

For the GT transitions of $^{22}\text{Mg} \rightarrow {}^{22}\text{Na}$, the observed strengths show a transient situation between the concentration and fragmentation of the GT transitions. Namely, the strength from $^{22}\text{Mg}(0_1^+ 1)$ is split into two final states, $^{22}\text{Na}(1_{1,2}^+ 0)$, in the low-energy region [5]. This may imply that a pn pair is formed in $^{22}\text{Na}(1_{1,2}^+ 0)$ but it is not the ideal deuteron-like pn pair. For the mirror nucleus, ^{22}Ne, a deformed core of the $^{16}\text{O} + \alpha$ cluster with two valence neutrons has been suggested by a theoretical study with the antisymmetrized molecular dynamics (AMD) [6–8]. ^{22}Mg may also have a prolately deformed nature with the spin-isospin saturated $^{16}\text{O} + \alpha$ cluster, and therefore the GT transitions of $^{22}\text{Mg} \rightarrow {}^{22}\text{Na}$ should be

dominantly contributed by the GT transitions of two nucleons at the surface of the deformed nuclei.

The pn pairing in deformed nuclei has been studied with mean-field approaches such as the generalized Hartree-Fock-Bogoliubov theories [9,10]. It was pointed out that, in medium-mass nuclei, the pairing correlations are reduced because of the nuclear deformation. Recently, the GT strengths of $^{24}\text{Mg}(0_1^+ 1) \rightarrow {}^{24}\text{Al}(1^+ 0)$ were studied by using the deformed quasiparticle random phase approximation (DQRPA) including pn pairing effects. [11] It was shown that the GT strengths are scattered in a broad energy region toward the high energy region by introducing the deformation. Such competitions between deformation and pn pairing should be investigated also in $N = Z$ odd-odd nuclei.

Our aim in this paper is to figure out the spin-isospin nature of the pn pairs in deformed nuclei by comparison between ^{10}B and ^{22}Na through analysis of the GT transition strengths. For this aim, we apply the method of T-projected antisymmetrized molecular dynamics with constraints on the deformation β and γ parameters ($T\beta\gamma$-AMD) [12] that can deal with pn correlations in $N = Z$ odd-odd nuclei and quadrupole deformations in light nuclei. We investigate the low-energy GT transitions of $^{22}\text{Ne} \rightarrow {}^{22}\text{Na}$. Particular attention is paid to the roles of the pn correlation in deformation effects on the fragmentation of the low-energy GT transitions from $^{22}\text{Ne}(0_1^+ 1)$, which have been observed in the mirror transitions $^{22}\text{Mg} \rightarrow {}^{22}\text{Na}$. We also investigate GT transitions between excited states in low-energy regions because discussions of the GT transitions between rotational band members are useful to understand pn correlation in the deformed system, though experimental data for such transitions are poor. It is also worthwhile to present systematic data of theoretical $B(\text{GT})$ values because they can be helpful for comparison with future experimental and theoretical works. In order to discuss universal features of the pn correlation in deformed nuclei and its effect on the GT transitions, we compare the GT transitions of $^{22}\text{Ne} \rightarrow {}^{22}\text{Na}$ with those of $^{10}\text{Be} \rightarrow {}^{10}\text{B}$.

The paper is organized as follows. The framework of the present calculation is explained in Sec. II, and the calculated results of nuclear properties of energy spectra, $B(M1)$, $B(E2)$, and $B(\text{GT})$, are shown in Sec. III. single-particle properties and dependence of $B(\text{GT})$ on deformation are discussed in Sec. IV. A summary and an outlook are given in Sec. V.

II. METHOD

A. $T\beta\gamma$-AMD

We applied the $T\beta\gamma$-AMD method to calculate ^{22}Na and ^{10}B transition strengths. The method was constructed in order to study pn correlations in $N = Z$ odd-odd nuclei, and applied for a study of GT transitions of ^{10}Be $\rightarrow$ ^{10}B. It is a useful approach to describe pn correlations in deformed nuclei because the method can control the isospin ($T = 0, 1$) and the collective deformation β and γ of $N = Z$ odd-odd nuclei, simultaneously. In this section, we briefly explain the mathematical formulations of $T\beta\gamma$-AMD. For detailed formulations, the reader is referred to Ref. [12].

$T\beta\gamma$-AMD is based on antisymmetrized molecular dynamics (AMD), in which Slater determinants of Gaussian wave packets are used as basis wave functions:

$$|\Phi(\beta, \gamma)\rangle = \mathcal{A}[|\phi_1\rangle|\phi_2\rangle \cdots |\phi_A\rangle], \quad (1)$$

$$|\phi_i\rangle = \left(\frac{2\nu}{\pi}\right)^{\frac{3}{4}} \exp\left[-\nu\left(r_i - \frac{Z_i}{\sqrt{\nu}}\right)^2\right]|\xi_i\rangle|\tau_i\rangle. \quad (2)$$

Here, we use $\nu = 0.16$ fm^{-2} for ^{22}Na, which reproduces radii of sd-shell nuclei. In order to obtain the optimized wave functions for parity (π) and isospin (T) eigenstates, the π and T projections are performed before energy variation:

$$|\Phi^{\pi T}(\beta, \gamma)\rangle = \hat{P}^\pi \hat{P}^T |\Phi(\beta, \gamma)\rangle, \quad (3)$$

where $\hat{P}^\pi$ and $\hat{P}^T$ are parity and isospin projection operators, respectively. For the $^{\pi T}$-projected wave function, we perform the energy variation under the constraints on the deformation parameters, β and γ, so as to obtain the optimized states corresponding to each (β, γ). After the variation, the obtained wave functions $|\Phi^{\pi T}(\beta, \gamma)\rangle$ are projected onto the total angular momentum J eigenstates: $\hat{P}^J_{MK}|\Phi^{\pi T}(\beta, \gamma)\rangle$. Here $\hat{P}^J_{MK}$ is the angular momentum projection operator. Furthermore, we superpose these $J^\pi T$ eigenstates over the (β, γ) plane with the generator coordinate method (GCM) to take into account the quantum fluctuations for quadrupole deformations:

$$\left|J^\pi_n T; M\right\rangle = \sum_{iK} c^{iK}_n \hat{P}^J_{MK} \left|\Phi^{\pi T}(\beta_i, \gamma_i)\right\rangle. \quad (4)$$

Here, the parameters β and γ are treated as generator coordinates in the GCM, and the K mixing is taken into account. We call this method $T\beta\gamma$-AMD+GCM.

B. Effective interactions

We use the Hamiltonian

$$H = K - K_{\text{cm}} + V_c + V_{LS} + V_{\text{Coulomb}}, \quad (5)$$
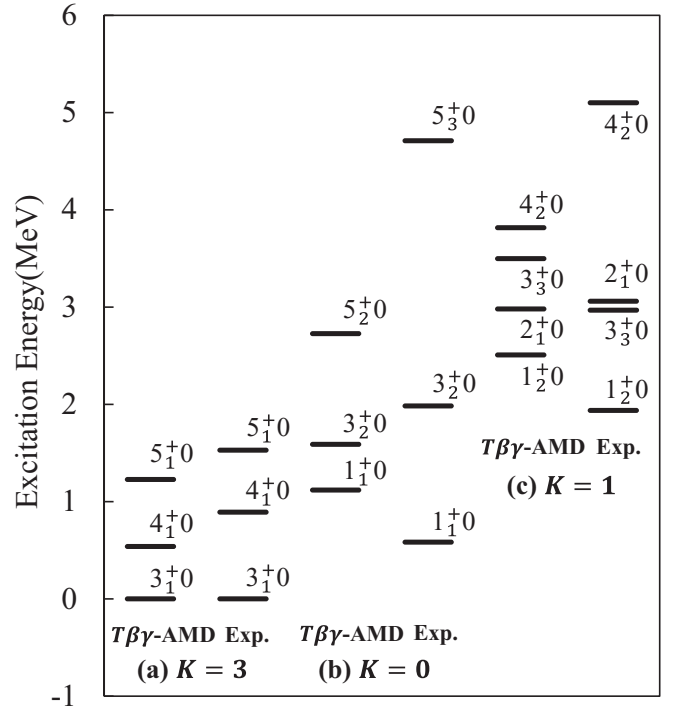

FIG. 1. The low-lying spectra of ^{22}Na in the $T = 0$, $K = 0, 1, 3$ bands. Calculated and experimental spectra are shown on the left and right, respectively. The experimental data are taken from [5].

where K is the kinetic energy, K_{cm} is the kinetic energy of the center of mass, and V_c, V_{LS}, and V_{Coulomb} are the central force, the spin-orbit force, and the Coulomb force, respectively. For the central force, the Volkov No. 2 force [13] with the Majorana exchange parameter $m = 0.6$ is used. The Bartlett and Heisenberg parameters $b = h = 0.06$ are adopted, which are phenomenologically adjusted to the energy difference between the lowest $T = 0$ and $T = 1$ states in ^{10}B [12]. For V_{LS}, we use the spin-orbit part of the G3RS force [14,15] with the same strength parameters $u_{ls} = u_1 = -u_2 = 1300$ MeV as those used in the previous works [12,16].

III. RESULTS

A. Energy spectra and electromagnetic transitions in ^{22}Na

The energy spectra for the $E < 8$ MeV states in ^{22}Na are shown in Figs. 1 and 2 and those in ^{22}Ne are shown in Fig. 3. The calculation reasonably reproduces low-lying energy spectra. In particular, the spectra of $J \leqslant 3$ states agree with the experimental data.

The $K = 0, 1$, and 3 bands are obtained in the isoscalar ($T = 0$) states of ^{22}Na. The ground band is the $K = 3$ band consisting of the $3^+_1 0$, $4^+_1 0$, and $5^+_1 0$ states. The calculated $E2$ transition strengths are shown in Table I together with the experimental data and shell-model calculation [17]. It should be noted that we use the bare charges in the present calculation instead of the effective charges which are usually used in shell-model calculations of the $E2$ transition strengths. As shown in the table, $E2$ transitions, $5^+_1 0 \rightarrow 4^+_1 0$, $4^+_1 0 \rightarrow 3^+_1 0$, and $5^+_1 0 \rightarrow 3^+_1 0$, in the $K = 3$ band are strong because of the
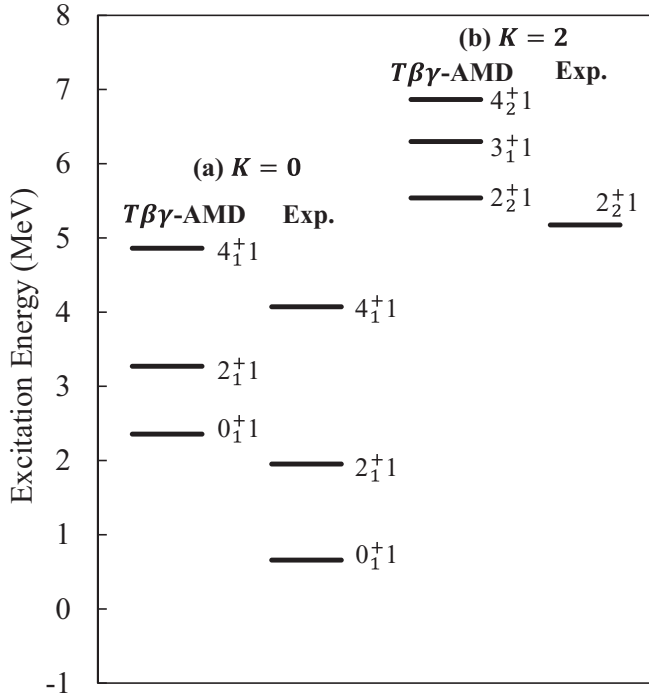
FIG. 2. The low-lying spectra of ^{22}Na in the $T = 1$, $K = 0, 2$ bands. For each band, calculated and experimental spectra are shown on the left and right, respectively. The experimental data are taken from [5].

prolate deformation, consistent with the experimental data. The bandhead 3_1^+0 obtained with the GCM has the largest overlap of 89.7% with the $J^\pi T = 3^+0$ and $K = 3$ projected
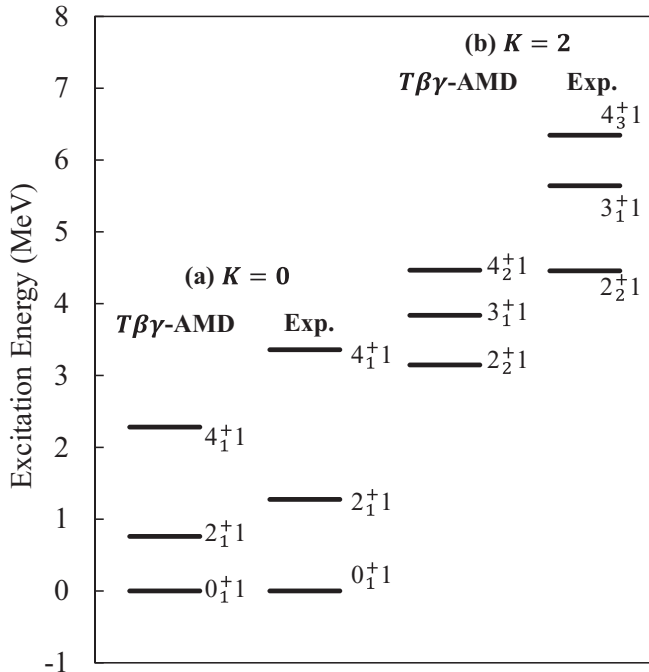

FIG. 3. The low-lying spectra of ^{22}Ne in the $K = 0, 2$ bands. For each band, calculated and experimental spectra are shown on the left and right, respectively. The experimental data are taken from [5].

TABLE I. The electric and magnetic moments and transition strengths in ^{22}Na. The calculated Q ($e\,\text{fm}^2$) and μ (μ_N) moments, $B(E2)$ ($e^2\,\text{fm}^4$), and $B(M1)$ (μ_N^2) are shown together with the experimental data from [5] and with the shell-model values from [17]. The binding energy (MeV) of the ground state ^{22}Na(3_1^+0) is also shown.

Observable	SM	$T\beta\gamma$-AMD +GCM	Exp.
binding energy		173.041	174.1456
$Q(3_1^+0)$		17.66	18.0(11)
$\mu(3_1^+0)$		1.784	1.746(3)
$\mu(1_1^+0)$		0.622	0.535(10)
$K = 3$			
$B(E2; 5_1^+0 \to 4_1^+0)$	76.9	49.9	58(18)
$B(E2; 4_1^+0 \to 3_1^+0)$	87.9	56.8	91(3)
$B(E2; 5_1^+0 \to 3_1^+0)$	20.1	12.0	19.0(15)
$B(M1; 4_2^+1 \to 5_1^+0)$		2.29	
$B(M1; 3_1^+1 \to 4_1^+0)$		3.35	
$B(M1; 2_2^+1 \to 3_1^+0)$		3.97	
$K = 0$			
$B(E2; 3_2^+0 \to 1_1^+0)$	65.9	35.5	69(7)
$B(E2; 5_2^+0 \to 3_2^+0)$	51.3	41.2	51(22); $5_3^+0 \to 3_2^+0$
$B(M1; 0_1^+1 \to 1_1^+0)$	5.37	5.00	4.96(18)
$B(M1; 2_1^+1 \to 3_2^+0)$		3.28	
$B(M1; 4_1^+1 \to 3_2^+0)$	2.33	0.27	>5.37
$B(M1; 4_1^+1 \to 5_2^+0)$	3.06	3.02	2.2(9); $4_1^+1 \to 5_3^+0$
$K = 1$			
$B(E2; 2_1^+0 \to 1_2^+0)$		43.9	
$B(E2; 3_3^+0 \to 2_1^+0)$		10.2	
$B(E2; 3_3^+0 \to 1_2^+0)$		13.9	
$B(E2; 4_2^+0 \to 3_3^+0)$		14.0	
$B(E2; 4_2^+0 \to 2_1^+0)$	65.9	24.4	
$B(M1; 0_1^+1 \to 1_2^+0)$	4.46	4.12	4.3(13)
$B(M1; 2_1^+1 \to 2_1^+0)$		2.21	1.22(16)
$K = 0, 1$ interband			
$B(E2; 2_1^+0 \to 1_1^+0)$		4.1	0.10(7)
$B(E2; 3_2^+0 \to 1_2^+0)$		1.7	
$B(E2; 1_1^+0 \to 1_2^+0)$		7.81	
$B(E2; 2_1^+0 \to 3_2^+0)$		9.42	

basis wave function, $\hat{P}_{M3}^{J=3}|\Phi^{+0}(\beta, \gamma)\rangle$, at $\beta = 0.29$ and $\gamma = 0.19$ on the β-γ plane, and shows the $K = 3$ nature of the deformed band. As discussed later, this band is understood as the deformed ^{20}Ne core with a spin-aligned pair of a proton and a neutron in the lowest valence orbit.

The 1_1^+0 state is the bandhead of the $K = 0$ band with the rotational band members 1_1^+0, 3_2^+0, and 5_2^+0 with the strong $E2$ transitions of $5_2^+0 \to 3_2^+0$ and $3_2^+0 \to 1_1^+0$. The experimental value of $B(E2; 3_2^+0 \to 1_1^+0)$ is consistent with the calculated value. For the 5_2^+0 state, we tentatively assign the experimental 5_3^+0 state because the experimental $B(E2; 5_3^+0 \to 3_2^+0)$ is of the same order as the calculated

value of $B(E2; 5_2^+0 \to 3_2^+0)$. The bandhead 1_1^+0 state has the largest overlap (82.7%) with the $J^\pi T = 1^+0$ and $K = 0$ projected wave function at $\beta = 0.31$ and $\gamma = 0.11$ and shows the $K = 0$ nature of the deformed band. Compared with the features of the ground $K = 3$ band, it can be seen that the $K = 0$ band has similar deformation but has different nature of the spin configuration of the valence proton and neutron.

The 1_2^+0 and 2_1^+0 states can be classified in the $K = 1$ band members because of the strong $E2$ transition and the $K = 1$ nature. The bandhead 1_2^+0 state has the largest overlap (76.6%) with the $J^\pi T = 1^+0$ and $K = 1$ projected wave function at $\beta = 0.29$ and $\gamma = 0.19$ and almost the same intrinsic deformation as those of the $K = 0$ and 3 bands.

It is worthwhile to discuss the interband $E2$ transitions to establish the $K = 0$ and 1 bands. The calculated $B(E2)$ values for the interband transitions $1_2^+0 \to 1_1^+0$, $2_1^+0 \to 3_2^+0$, $2_1^+0 \to 1_1^+0$, and $1_2^+0 \to 3_2^+0$ between $K = 0$ and 1 bands are generally small. The experimental data of $B(E2; 2_1^+0 \to 1_1^+0)$ are small and support our results.

The $M1$ transition is a good probe for spin configuration because it is contributed by the spin flip transitions. Similarly to the GT transitions, the isovector $M1$ transitions from $T = 1$ states are useful observables for spin structure in $T = 0$ states. In Table I, the calculated strengths of the isovector $M1$ transitions in ^{22}Na are shown together with the experimental data. In the table, the theoretical values of the shell-model calculation [17] are also shown. The $B(M1)$ values of the present calculation are qualitatively similar to the shell model values except for the $B(M1; 4_1^+1 \to 3_2^+0)$. The observed strong $M1$ transitions from the $T = 1$, $K = 0$ bands are described well by the present calculation except for $B(M1; 4_1^+1 \to 3_2^+0)$. The calculated $B(M1; 4_1^+1 \to 5_2^+0)$ in our calculation is comparable with the experimental $B(M1; 4_1^+1 \to 5_3^+0)$. It supports our assignment of the calculated 5_2^+0 state to the experimental 5_3^+0 state. For the transition $4_1^+1 \to 3_2^+0$, the present calculation underestimates the experimental $B(M1)$.

B. Gamow-Teller transitions and SU(4) symmetry

The GT transition operator is given as

$$B(\mathrm{GT}) = \frac{1}{2J_i + 1} \left| \left\langle J_f \left\| \sum_i \sigma^i \tau_\pm^i \right\| J_i \right\rangle \right|^2, \quad (6)$$

which changes the spin and isospin of the initial state to $\Delta S = 1$ and $\Delta T = 1$, and is regarded as the rotation operator in the spin and isospin SU(4) space. In the previous work [16], we investigated the GT transitions of ^{10}Be $\to$ ^{10}B and discussed the spin-isospin partner states connected with strong GT transitions in ^{10}Be and ^{10}B. For the assigned partner states, the initial and final states are described by the $S = 0$, $T = 1$ nn and $S = 1$, $T = 0$ pn pairs of two valence nucleons around the 2α core, respectively. This means that the strong GT transitions are understood by the transitions of the NN pairs with approximate SU(4) symmetry in the spin and isospin space. The SU(4) symmetry of the NN pair is partially broken in ^{22}Na, because the intrinsic spin of the NN pairs strongly couples to the core deformation because of the spin-orbit mean potential, and therefore the symmetry of the

TABLE II. The GT transition strengths defined by Eq. (6). of ^{22}Ne $\to$ ^{22}Na. The experimental data are taken from [5].

Observable	$T\beta\gamma$-AMD+GCM	Exp.
$K = 2 \to K = 3$		
$B(\mathrm{GT}; 4_2^+1 \to 5_1^+0)$	0.95	
$B(\mathrm{GT}; 3_1^+1 \to 4_1^+0)$	1.27	
$B(\mathrm{GT}; 2_2^+1 \to 3_1^+0)$	1.51	
$K = 0 \to K = 0$		
$B(\mathrm{GT}; 0_1^+1 \to 1_1^+0)$	1.98	(0.949(28))
$B(\mathrm{GT}; 2_1^+1 \to 1_1^+0)$	0.30	
$B(\mathrm{GT}; 2_1^+1 \to 3_2^+0)$	1.24	
$B(\mathrm{GT}; 4_1^+1 \to 5_2^+0)$	1.12	
$K = 0 \to K = 1$		
$B(\mathrm{GT}; 0_1^+1 \to 1_2^+0)$	1.55	(1.43(8))
$B(\mathrm{GT}; 2_1^+1 \to 1_2^+0)$	0.37	
$B(\mathrm{GT}; 2_1^+1 \to 2_1^+0)$	0.82	
$B(\mathrm{GT}; 4_1^+1 \to 3_2^+0)$	0.12	
$K = 0 \to K = 3$		
$B(\mathrm{GT}; 2_1^+1 \to 3_1^+0)$	0.0015	0.00022

spin rotation is broken. Nevertheless, we can also assign the spin-isospin partners in the GT transitions of ^{22}Ne $\to$ ^{22}Na for the subspaces of the final states, which are separated by the deformation effect. Below, we discuss the GT transitions and assignments of spin-isospin partners in ^{22}Ne $\to$ ^{22}Na.

The calculated GT transitions of ^{22}Ne $\to$ ^{22}Na are shown in Table II. We obtained the significant GT transition strengths from the $K = 0$ and $K = 2$ bands of ^{22}Ne to the $K = 0$, $K = 1$, and $K = 3$ bands of ^{22}Na.

The GT transition strengths from the $K = 0$ band states of ^{22}Ne are split into the $K = 0$ and $K = 1$ band states of ^{22}Na. The GT transition strengths from the 0_1^+1 are fragmented into two low-lying 1^+0 states, ^{22}Na(1_1^+0) and ^{22}Na(1_2^+0). The result is consistent with the experimental observations for the mirror transitions ^{22}Mg(0_1^+1) $\to$ ^{22}Na($1_{1,2}^+0$)). Also, for the transitions from the initial 2_1^+1, we obtain the GT strengths fragmented into 2_1^+0 and 3_2^+0. These final states in the $K = 0$ and $K = 1$ bands in ^{22}Na are regarded as spin-isospin partners of the initial $K = 0$ band states in ^{22}Ne. As we show in detail later, the K quanta, $K = 0$ and $K = 1$, of the final states in ^{22}Na are mainly contributed by the intrinsic spin of the $T = 0$, $S = 1$ pn pair; $S_z = \pm 1$ contributes to $K = \pm 1$ and $S_z = 0$ corresponds to $K = 0$. The GT transitions into the former and the latter bands occur by the spin flip $\sigma_\pm \propto \sigma_x \pm i\sigma_y$ with $\Delta S_z = \pm 1$ and nonflip operators σ_0 with $\Delta S_z = 0$, respectively, because the initial state in the $K = 0$ band has the dominant $S_z = 0$ component. This means that the splitting of the GT transition strengths is a consequence of the formation of two low-lying bands, $K = 0$ and $K = 1$, because of the $T = 0$, $S = 1$ pn pair correlation in the deformed system. In other words, because of the symmetry breaking of the spin rotation of the $T = 0$, $S = 1$ pn pair in ^{22}Na, the GT transition strengths from ^{22}Ne(0_1^+1) do not concentrate to a single 1^+0 state. It is a different situation from

TABLE III. The single-particle properties of the major component of the ^{22}Na($3^+_1 0$) ground state at $(\beta, \gamma) = (0.29, 0.19)$. The column labeled "parity" stands for the fraction of positive parity component in each single-particle state.

Neutron						Proton						Shell
Energy	$\langle \hat{j}^2 \rangle$	$\langle \hat{\ell}^2 \rangle$	Parity	Ω	Λ	Energy	$\langle \hat{j}^2 \rangle$	$\langle \hat{\ell}^2 \rangle$	Parity	Ω	Λ	
−60.94	0.75	0.00	1.00	0.50	0.02	−55.98	0.75	0.00	1.00	0.50	0.02	$s_{1/2}$
−59.29	0.75	0.00	1.00	0.50	0.03	−54.38	0.75	0.00	1.00	0.50	0.02	
−38.17	3.25	2.03	0.00	0.51	0.21	−33.64	3.26	2.05	0.00	0.51	0.22	$p_{3/2}$
−36.60	3.29	2.03	0.00	0.52	0.23	−32.16	3.38	2.03	0.00	0.52	0.26	
−32.13	3.70	2.07	0.00	1.48	1.00	−27.66	3.65	2.09	0.00	1.46	1.01	
−31.12	3.72	2.08	0.00	1.47	1.00	−26.63	3.75	2.09	0.00	1.48	1.00	
−27.61	1.53	2.19	0.00	0.63	1.00	−23.66	1.39	2.03	0.00	0.63	0.98	$p_{1/2}$
−26.26	1.50	2.08	0.00	0.59	0.99	−21.80	1.48	2.09	0.00	0.61	1.00	
−18.37	5.42	4.07	0.97	0.56	0.31	−14.14	5.81	4.25	0.97	0.60	0.34	α in sd shell
−17.25	6.12	4.46	0.98	0.60	0.39	−13.07	5.90	4.30	0.97	0.62	0.39	
−11.26	7.36	5.75	0.96	1.33	1.06	−7.29	7.32	5.77	0.98	1.38	1.05	$\approx [211\,3/2]$

the super-allowed GT transitions of ^{6}Li and ^{10}B, in which the spin $S = 1$ of the pn pair couples weakly with the core and approximately maintains the SU(4) symmetry.

For the GT transition to the ground $K = 3$ band in ^{22}Na, the strong GT transitions from the $K = 2$ band in ^{22}Ne are obtained: the strengths from the initial states $2^+_2 1$, $3^+_1 1$, and $4^+_2 1$ concentrate into the final states $3^+_1 0$, $4^+_1 0$, and $5^+_1 0$, respectively. In the initial states, the quanta $K = 2$ are given by the orbital angular momenta of the valence $S = 0$ nn pair. The $K = 3$ of the final states are described by the orbital angular momentum $L_z = 2$ and the spin $S = 1$ of the pn pair aligned to the z direction of the deformed intrinsic state because of the spin-orbit mean potential. The GT transitions $K = 2 \rightarrow K = 3$ occur as the transition $S = 0$ $nn \rightarrow T = 0$, $S = 1$ pn with $\Delta S = 1$ by the spin flip operator $\sigma_\pm$. Therefore, the $K = 3$ states in ^{22}Na are assigned to spin-isospin partners of the $K = 2$ states in ^{22}Ne.

IV. DISCUSSION

In this section, we analyze single-particle orbits of valence protons and neutrons in ^{22}Na and compare the GT transitions of ^{22}Ne $\rightarrow$ ^{22}Na with those of ^{10}Be $\rightarrow$ ^{10}B.

A. Single-particle orbit and Nilsson diagram

We discuss single-particle properties of the $K = 0, 1, 3$ bands of ^{22}Na analyzing the major components of the band-head states. In Table III, we show single-particle properties of the intrinsic wave function at $(\beta, \gamma) = (0.29, 0.19)$, which is the dominant component of the ground $3^+_1 0$ state for the $K = 3$ band. The single-particle energies, the expectation values of squared angular momenta and orbital angular momenta, and positive parity probabilities are shown. In order to discuss the link with Nilsson orbits, we also show the Ω and Λ values for each single-particle orbit,

$$\Omega = \sqrt{\langle \phi_i^{\text{s.p.}} | \hat{j}_z^2 | \phi_i^{\text{s.p.}} \rangle}, \tag{7}$$

$$\Lambda = \sqrt{\langle \phi_i^{\text{s.p.}} | \hat{\ell}_z^2 | \phi_i^{\text{s.p.}} \rangle}. \tag{8}$$

The lower 20 orbits for 10 protons and 10 neutrons form the ^{20}Ne core, and the last two orbits correspond to the valence proton and neutron around it. In the ^{20}Ne core, the four nucleons in the sd shell are not in the ideal $d_{5/2}$ orbits, but they form an α cluster at the surface of ^{16}O. As a result, the intrinsic states of ^{22}Na is well deformed. The four nucleons in the α cluster do not contribute to the GT transitions because they form a spin-isospin saturated state. It is a different feature from the case of four nucleons in the lowest Nilsson orbits in the $N = 2$ shell in a deformed mean field.

On the other hand, the single-particle properties of the last two valence nucleons around the ^{20}Ne core show nature of the spin-orbit favored Nilsson $[Nn_z \Lambda\Omega] = [211\,3/2]$ orbit in prolate deformation. In the $T = 0$ states, the $K = 3$ band is the lowest because two $[211\,3/2]$ nucleons in the intrinsic spin $S = 1$ state feel the attraction of the triplet-even nuclear interaction. Thus, the intrinsic structure of the ground $K = 3$ band of ^{22}Na is simply described by the ^{20}Ne core with two valence neutrons in the $[211 + 3/2]^p [211 + 3/2]^n$ configuration.

The deformation and single-particle properties of the intrinsic states of $K = 0$ and $K = 1$ bands are similar to those of the $K = 3$ band. Also in the $K = 0$ and $K = 1$ bands, the ^{20}Ne core is formed by the lower 20 orbits for 10 protons and 10 neutrons. The last two orbits for the valence proton and neutron around the core have the dominant $[211 + 3/2]$ component, but they also contain other minor components such as the $[211 − 3/2]$ and $[211 − 1/2]$ orbits. The $K = 0$ and $K = 1$ bands are produced from these minor components by the J^π and K projections. Namely, the $1^+_1 0$ ($K = 0$) state contains the $[211 + 3/2]^{p(n)} [211 − 3/2]^{n(p)}$ configuration of two nucleons coupling to $S = 1$ with $S_z = 0$. On the other hand, the $1^+_2 0$ ($K = 1$) state is regarded as the $[211 + 3/2]^{p(n)} [211 − 1/2]^{n(p)}$ configuration of two nucleons with $S_z = 1$.

With a similar analysis of the single-particle orbits for ^{22}Ne, the intrinsic state of ^{22}Ne($0^+_1 1$) is described by two $[211\,3/2]$-orbit neutrons in the $[211 + 3/2]^n [211 − 3/2]^n$ configuration with $K = 0$ around the ^{20}Ne core.

In the single-particle analysis, it is found that the structures of the low-lying states of ^{22}Ne and ^{22}Na are approx-
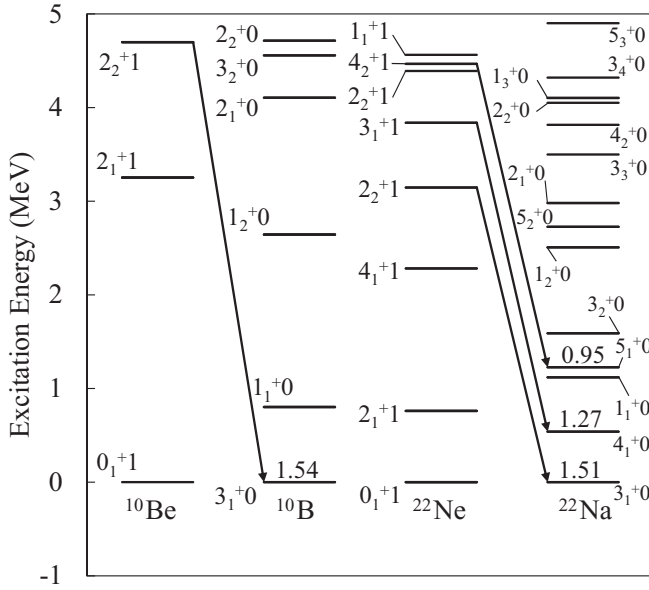
FIG. 4. The GT transitions $K = 2 \rightarrow K = 3$ with large B(GT) values are shown with solid arrows. The energy is measured from each ground state.

FIG. 5. The spectra of initial and final states in ^{10}Be $\rightarrow$ ^{10}B($T = 0$). The energy is measured from each ground state. The states having large B(GT) are connected by arrows.

imately described by Nilsson orbit configurations of two valence nucleons around the deformed ^{20}Ne core, which we call the "$\Omega\Omega$-coupling scheme" in this paper. The GT transitions from ^{22}Ne(0_1^+1) to ^{22}Na($1_{1,2}^+0$) are mainly contributed by the transitions of two valence neutrons, $nn \rightarrow pn$, around the ^{20}Ne core. In the $0_1^+1 \rightarrow 1_1^+0$ transition two valence neutrons $|n\uparrow n\downarrow\rangle$ decay into $|p\uparrow n\downarrow\rangle$ with $\Delta S_z = 0$, whereas in the $0_1^+1 \rightarrow 1_2^+0$ transition they decay into $|p\downarrow n\downarrow\rangle$ with $\Delta S_z = \pm 1$. In the $\Omega\Omega$-coupling scheme, the former $\Delta S_z = 0$ and the latter $\Delta S_z = \pm 1$ transitions correspond to $[211 + 3/2]^n[211 - 3/2]^n \rightarrow [211 + 3/2]^{p(n)}[211 - 3/2]^{n(p)}$ and $[211 + 3/2]^n[211 - 3/2]^n \rightarrow [211 + 3/2]^{p(n)}[211 - 1/2]^{n(p)}$, respectively. Thus, the GT transition from ^{22}Ne(0_1^+1) is split into the spin nonflip and flip states in ^{22}Na.

B. Comparison of GT transitions of ^{10}Be $\rightarrow$ ^{10}B and ^{22}Ne $\rightarrow$ ^{22}Na

In order to give more general discussions of the low-energy GT transitions in deformed systems, we compared the GT transitions of ^{22}Ne $\rightarrow$ ^{22}Na with those of ^{10}Be $\rightarrow$ ^{10}B studied with the same method in the previous work [16], because ^{10}Be and ^{10}B are also deformed nuclei in the p shell with two valence nucleons around the 2α core. In ^{10}Be $\rightarrow$ ^{10}B, the strong GT transitions occur in two valence nucleons from a nn pair to a pn pair around the core.

In Figs. 4 and 5, the energy spectra and B(GT) values in ^{10}Be and ^{10}B calculated with the $T\beta\gamma$-AMD+GCM are shown. The GT transitions are strong in ^{10}Be(0_1^+1) $\rightarrow$ ^{10}B(1_1^+0), ^{10}Be(2_1^+1) $\rightarrow$ ^{10}B($1_2^+0, 2_{1,2}^+0, 3_2^+0$), and ^{10}Be($2_2^+1$) $\rightarrow$ ^{10}B(3_1^+0). The initial states of ^{10}Be are in the $K = 0$ or $K = 2$ band. The final states in ^{10}B are regarded
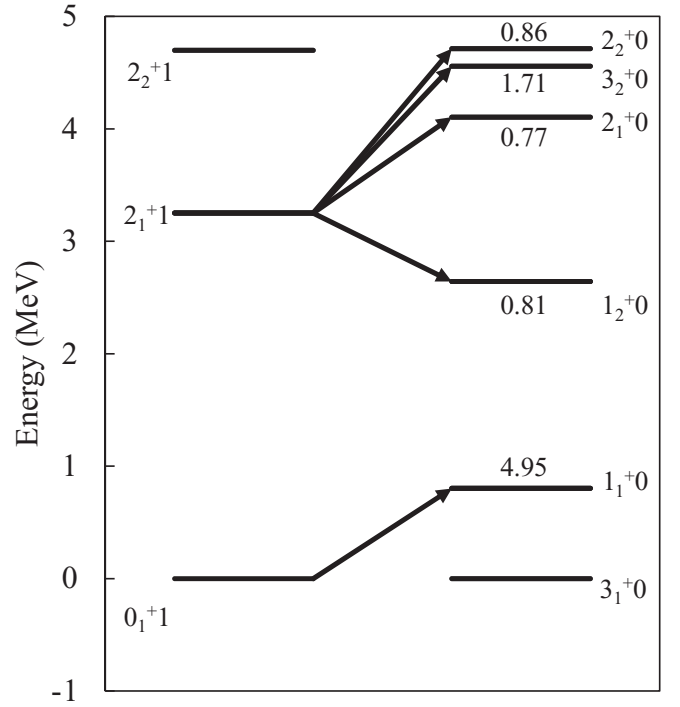
as the spin-isospin partner states of the $K = 0$ or $K = 2$ band members in ^{10}Be, as discussed in the previous paper [16].

The strong GT transition ^{10}Be(2_2^+1) $\rightarrow$ ^{10}B(3_1^+0) is regarded as the transition from the $K = 2$ sideband to the ground $K = 3$ band, which corresponds well to the GT transition of ^{22}Ne(2_2^+1) $\rightarrow$ ^{22}Na(3_1^+0). On the other hand, the GT transitions from the $K = 0$ ground band of ^{10}Be show different features from those of ^{22}Ne. The GT transition from ^{10}Be(0_1^+1) is not split but concentrated on the single ^{10}B(1_1^+0) state because the final states in ^{10}B do not have definite K quanta even though they have the deformed 2α core with two valence nucleons. Instead, they have spatially developed deuteron-like pn pairs weakly coupling with the 2α core in the "LS-coupling" scheme rather than the $\Omega\Omega$-coupling scheme.

In order to see spatial correlations of NN pairs, we visualized the spatial distribution of the $S = 1$, $T = 0$ and $S = 0$, $T = 1$ NN pairs with two-particle density $\rho_{ST}(r)$ defined as

$$\rho_{ST}(r) = \frac{\langle \Phi^T(\beta, \gamma) | \hat{\rho}_{ST}(r) | \Phi^T(\beta, \gamma) \rangle}{\langle \Phi^T(\beta, \gamma) | \Phi^T(\beta, \gamma) \rangle}, \quad (9)$$

$$\hat{\rho}_{ST}(r) \equiv \sum_{ij} \hat{P}_{ij}^S \hat{P}_{ij}^T \delta(r - \hat{r}_i) \delta(r - \hat{r}_j), \quad (10)$$

where $\hat{P}_{ij}^S$ and $\hat{P}_{ij}^T$ are the spin and isospin projection operators for two nucleons [16]. In Fig. 6, we show $\rho_{NN}(r) \equiv \rho_{10}(r) - \rho_{01}(r)$ for the major components of ^{10}Be, ^{10}B, ^{22}Ne, and ^{22}Na. Here, $\rho_{01}(r)$ is subtracted to cancel contributions from the core nuclei. In ^{10}Be and ^{10}B, the 2α cluster is elongated along the z axis, as seen in Figs. 6(a)
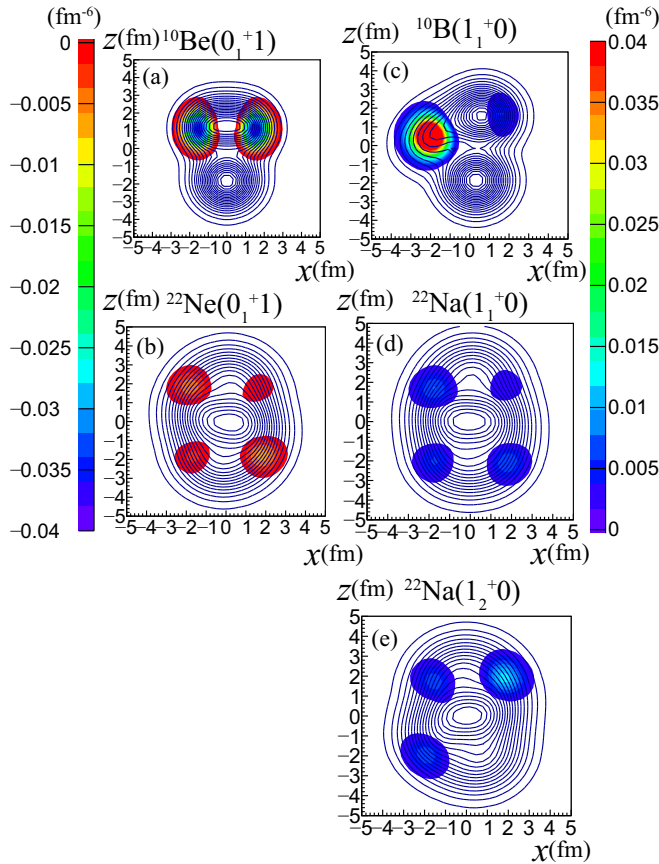
FIG. 6. The two-nucleon-pair density $\rho_{NN}(\boldsymbol{r})$ of (a) ^{10}Be(0_1^+1), (b) ^{22}Ne(0_1^+1), (c) ^{10}B(1_1^+0), (d) ^{22}Na(1_1^+0), and (e) ^{22}Na(1_2^+0). The one-body density distribution $\rho(r)$ is also shown by (blue) solid contour lines.

FIG. 7. The spectra of initial and final states in ^{22}Ne $\rightarrow$ ^{22}Na($T = 0$). The energy is measured from each ground state. The states having large B(GT) are connected by arrows. The solid arrows are $K = 0 \rightarrow K = 0$ transitions and the dashed arrows are $K = 0 \rightarrow K = 1$ ones.

and 6(c). In the ^{10}B(1_1^+0), the $T = 0$ pn pair distribution has a remarkable peak at $(x, z) = (-2, 0)$ (fm) and shows the spatially developed deuteron-like pn pair far from the 2α core. In contrast, the nn and pn pairs in ^{22}Ne and ^{22}Na are distributed at the surface of the deformed core and show no spatial development.

As a result of the 2α cluster formation and the spatial development of the deuteron-like pn pair, the $1_{1,2}^+0$, $2_{1,2}^+0$, 3_2^+0 states of ^{10}B are constructed by the coupling of the $S = 1$ pn pair with orbital angular momentum L of the 2α core as $[L = 0, S = 1]_{J=1}$ and $[L_{core} = 2, S = 1]_{J=1,2,3}$. Here, both $2_{1,2}^+0$ states contain $[L_{core} = 2, S = 1]_{J=2}$ component because of the configuration mixing between the core rotation $L_{core} = 2$ and pn pair rotation $L_{pn} = 2$ in the $J = 2$ state [16]. The strong GT transition ^{10}Be(0_1^+1) $\rightarrow$ ^{10}B(1_1^+0) corresponds to $[L = 0, S = 0]_{J=0} \rightarrow [L = 0, S = 1]_{J=1}$, whereas the significant GT transitions of ^{10}Be(2_1^+1) $\rightarrow$ ^{10}B($1_2^+0, 2_{1,2}^+0, 3_2^+0$) are described by the transitions $[L_{core} = 2, S = 0]_{J=2} \rightarrow [L_{core} = 2, S = 1]_{J=1,2,3}$. In ^{10}B, the intrinsic spin of the LS-coupling pn pair weakly couples with the core deformation. In such a case, the GT transition from the ground state ^{10}Be(0_1^+1) is not split but concentrated on the single state ^{10}B(1_1^+0) because both the spin flip and nonflip operators in the GT transition operator can contribute to the same final state. This
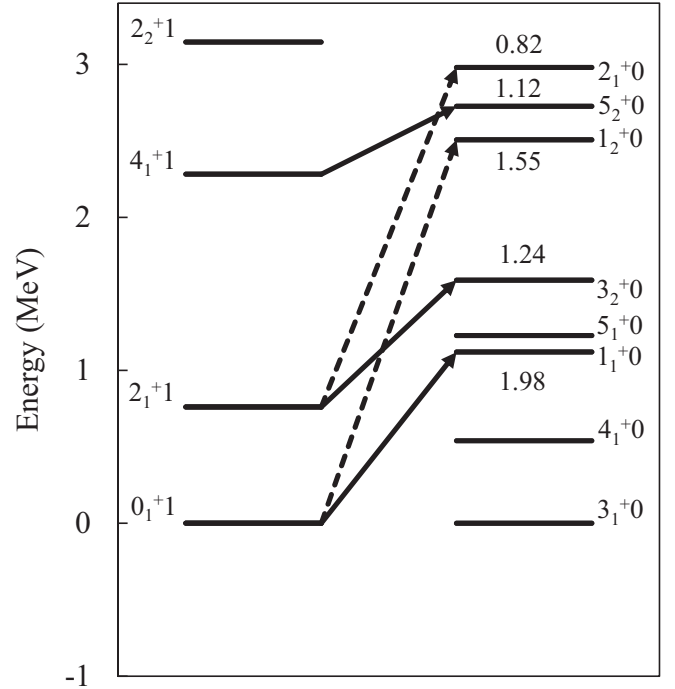
is a consequence of the SU(4) symmetry of the LS-coupling pn pair in ^{10}B.

Differently from the GT transition of ^{10}Be(0_1^+1) $\rightarrow$ ^{10}B(1_1^+0), the GT splitting occurs in ^{22}Ne(0_1^+1) $\rightarrow$ ^{22}Na($1_{1,2}^+0$) (see Fig. 7). As already discussed previously, the origin of the splitting is that the final states of ^{22}Na have specific K quanta because of the $\Omega\Omega$-coupling pn pair around the ^{20}Ne core. The GT transitions to the final $K = 1$ and $K = 0$ bands occur in the $nn \rightarrow pn$ decays with $\Delta S_z = 0$ and $\Delta S_z = \pm1$ in the intrinsic frames, respectively. The key point is that ^{22}Na($1_{1,2}^+0$) have the $\Omega\Omega$-coupling pn pair with the SU(4)-symmetry breaking, and ^{10}B(1_1^+0) has the LS-coupling pn pair with SU(4) symmetry.

In order to discuss the roles of pn correlation and core deformation in the GT splitting (or fragmentation) phenomena, we performed a further analysis of the GT transitions for the artificially prepared final states with the pn pairs around deformed cores in the LS-coupling limit and in the $\Omega\Omega$-coupling case, and in the jj-coupling limit. To this end, we changed the strength u_{ls} of the spin-orbit interaction V_{LS} to $u_{ls} = \lambda u_{ls}^{default}$ with the enhancement factor λ from the default strength $u_{ls}^{default} = 1300$ MeV, and performed the GCM calculation of ^{10}B and ^{22}Na. In the GCM calculation, we used the bases $\{|\Phi^{\pi T}(\beta_i, \gamma_i)\rangle\}_i$ obtained with the default spin-orbit strength. The $u_{ls} \rightarrow 0$ limit corresponds to the LS-coupling scheme with SU(4) symmetry, whereas in the large-u_{ls} limit the system goes to spherical states with jj-coupling nucleons. In the intermediate case of u_{ls}, $\Omega\Omega$-coupling NN pairs appear
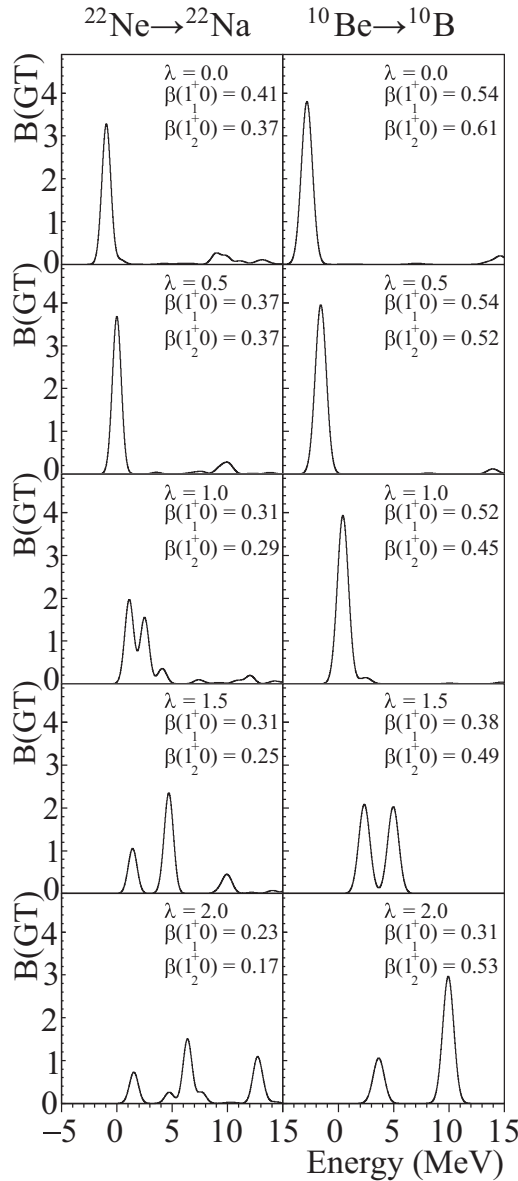
FIG. 8. The $B(GT)$ spectra obtained by calculations with the modified spin-orbit strengths with $\lambda = 0.0, 0.5, 1.0, 1.5, 2.0$. $\lambda = 1.0$ corresponds to the default strength. Each spectrum is smeared by a Gaussian with $\sigma = 0.4$ so as to normalize the peak hight to the $B(GT)$ value for the case of an isolated peak. For each λ, the energies are measured from ^{22}Na(3_1^+0) and ^{10}B(3_1^+0), respectively. The left and right panels show $B(GT; {}^{22}$Ne $\to {}^{22}$Na$)$ and $B(GT; {}^{10}$Be $\to {}^{10}$B$)$, respectively.

around the deformed core. By controlling the enhancement factor in the range of $\lambda = 0$–2, we discuss how the GT transitions are fragmented in the change from the LS-coupling regime to the jj-coupling regime.

In Fig. 8, we show the $B(GT; {}^{22}$Ne$(0_1^+1) \to {}^{22}$Na$(1_n^+0))$ spectra for $\lambda = 0.0, 0.5, 1.0, 1.5,$ and 2.0 in comparison with the $B(GT; {}^{10}$Be$(0_1^+1) \to {}^{10}$B$(1_n^+0))$ spectra. Let us first discuss the GT transitions of ^{22}Ne$(0_1^+1) \to {}^{22}$Na(1_n^+0). In the $\lambda = 0.0$ case for the LS-coupling limit, the pn pair has SU(4) symmetry and the GT strength is concentrated on the

single lowest state with a large fraction 54.8% of the GT sum rule value 6. As λ increases, the GT strengths from ^{22}Ne(0_1^+1) are split into a few 1^+0 states in the low-energy region. At the default strength $\lambda = 1.0$, the LS-coupling pn pair around the ^{20}Ne changes to the $\Omega\Omega$-coupling pair, and the GT strengths are split mainly to two states ^{22}Na$(1_{1,2}^+0)$. Significant GT strengths still exist in the low-energy region: The sum of the strengths for these two states exhausts 58.8% of the sum rule value. This corresponds to partial breaking of the SU(4) symmetry in sd-shell nucleons because this symmetry is broken only in the pn pairs but not in the α cluster. With further increase of λ to $\lambda = 2.0$, the deformation parameter becomes small as $\beta = 0.31 \to 0.23$ and the GT strengths are fragmented into many 1^+0 states. The major peak position rises up to the higher energy and the strength function is widely distributed. In the large-λ case, the α cluster is broken by the strong spin-orbit force and the system goes to the jj-coupling regime, in which six nucleons in the sd shell contribute to the GT transitions.

Next we look into the $B(GT; {}^{10}$Be$(0_1^+1) \to {}^{10}$B$(1_n^+0))$ spectra and compare them with ^{22}Ne$(0_1^+1) \to {}^{22}$Na(1_n^+0). Also, in ^{10}Be$(0_1^+1) \to {}^{10}$B(1_n^+0), we find similar behavior of the GT splitting with the SU(4)-symmetry breaking. In the small-λ case for the LS-coupling limit, the GT strength from ^{10}Be(0_1^+1) is concentrated on ^{10}B(1_1^+0) with $B(GT) \approx 5.0$ which almost exhausts the sum rule value because of the SU(4) symmetry of the NN pair around the 2α core. As λ increases, the GT peak is split into two states $1_{1,2}^+0$ and shifted toward the high-energy region. One of the remarkable differences from ^{22}Ne$(0_1^+1) \to {}^{22}$Na(1_n^+0) is that, in the case of ^{10}Be$(0_1^+1) \to {}^{10}$B(1_n^+0), the splitting occurs not at $\lambda = 1.0$ (the default spin-orbit strength) but at $\lambda = 1.5$ because the NN pairs around the 2α core favor the LS-coupling scheme. This means that, in the realistic system at $\lambda = 1.0$, the SU(4) symmetry in the pn pair still remains and the GT transition is concentrated on the single low-lying ^{10}B(1_1^+0).

In the present analysis, we found a universal feature of the GT fragmentation phenomena in deformed systems. There are two types of the fragmentation mechanism of the GT strengths. One is the GT splitting in the $K = 0, 1$ bands because of the SU(4)-symmetry breaking in the pn pairs around a largely deformed core with the spin-isospin saturated configurations. This corresponds to the partial breaking of the SU(4) symmetry. The other is the GT fragmentation in jj-coupling shell orbits in the weakly deformed system. ^{22}Ne$(0_1^+1) \to {}^{22}$Na$(1_{1,2}^+0)$ is the former case of the partial breaking phase, whereas ^{10}Be$(0_1^+1) \to {}^{10}$B(1_1^+0) is close to the ideal SU(4)-symmetry phase with no GT splitting.

V. SUMMARY AND OUTLOOK

We have investigated the Gamow-Teller transitions of ^{22}Ne $\to {}^{22}$Na with $T\beta\gamma$-AMD+GCM in order to discuss the relation between strong GT transitions and pn pair formation in prolately deformed $N = Z$ odd-odd nuclei. The splitting of the GT strengths from ^{22}Ne$(0_1^+1) \to {}^{22}$Na$(1_{1,2}^+0)$ is found, reproducing the experimental data in the mirror transitions, ^{22}Mg$(0_1^+1) \to {}^{22}$Na$(1_{1,2}^+0)$. This GT splitting is understood by introducing the "$\Omega\Omega$-coupling scheme" of the valence NN

pair around the spin-isospin saturated ^{20}Ne core. By analyzing the major components of the K bandheads, we have found that the final states $(1_1^+0, 3_2^+0, 5_2^+0)$ are in the $K = 0$ band and other states $(1_2^+0, 2_1^+0)$ are in the $K = 1$ band. The single-particle orbits for the two valence particles of the 1_1^+0 ($K = 0$) state show that this K quantum is produced by the $[211 + 3/2]^{p(n)}[211 - 3/2]^{n(p)}$ configuration with the intrinsic spins coupled to $S = 1$ with $S_z = 0$. On the other hand, those of the 1_2^+0 ($K = 1$) state have the major $[211 + 3/2]^{p(n)}[211 - 1/2]^{n(p)}$ configuration with $S_z = \pm 1$. This fact shows that the GT splitting is caused by the SU(4)-symmetry breaking of the pn pair into the $\Omega\Omega$-coupling scheme producing K quanta in the intrinsic frame. For the final states in the $K = 0$ and $K = 1$ bands with the $S_z = 0$ and $S_z = \pm 1$ pn pairs, the GT transitions occur in the $nn \to pn$ decays with $\Delta S_z = 0$ (spin nonfilpflip) and $S_z = \pm 1$ (spin flip) in the intrinsic frame, respectively.

We have also compared the GT transitions in ^{22}Ne $\to$ ^{22}Na with those in ^{10}Be $\to$ ^{10}B. The GT splitting in ^{22}Ne$(0_1^+1) \to$ ^{22}Na$(1_{1,2}^+0)$ occurs as a result of the SU(4)-symmetry breaking in the pn pair around a largely deformed core with the spin-isospin saturated configurations. On the other hand, ^{10}Be$(0_1^+1) \to$ ^{10}B(1_1^+0) is close to the SU(4)-symmetry phase with no GT splitting because the pn pair in ^{10}B is spatially developed and contains both the $K = 0, 1$ quanta, though the 2α core is also deformed.

The experimental study to measure B(GT) for ^{22}Ne$(0_1^+1) \to$ ^{22}Na(1^+0) at the Research Center for Nuclear Physics (Osaka) is ongoing and new data will come in the future. For other transitions, it is difficult to experimentally measure B(GT) because of limitations of present facilities. Instead, experimental measurements of $B(M1)$ values are needed as alternative probes for the pn correlation because $B(M1)$ values shown in this paper have good correspondence with the GT strengths. Moreover, further theoretical and experimental studies of the GT transitions for other $Z = N$ odd-odd nuclei are also important for understanding universal features of pn correlation in a deformed system.

[1] S. Frauendorf and A. O. Macchiavelli, Prog. Part. Nucl. Phys. **78**, 24 (2014).

[2] Y. Tanimura, H. Sagawa, and K. Hagino, Prog. Theor. Exp. Phys. **2014**, 053D02 (2014).

[3] Y. Fujita, H. Fujita, T. Adachi, G. Susoy, A. Algora, C. L. Bai, G. Colò, M. Csatlós, J. M. Deaven, E. Estevez-Aguado, C. J. Guess, J. Gulyás, K. Hatanaka, K. Hirota, M. Honma, D. Ishikawa, A. Krasznahorkay, H. Matsubara, R. Meharchand, F. Molina, H. Nakada, H. Okamura, H. J. Ong, T. Otsuka, G. Perdikakis, B. Rubio, H. Sagawa, P. Sarriguren, C. Scholl, Y. Shimbara, E. J. Stephenson, T. Suzuki, A. Tamii, J. H. Thies, K. Yoshida, R. G. T. Zegers, and J. Zenihiro, Phys. Rev. C **91**, 064316 (2015).

[4] Y. Fujita *et al.*, Phys. Rev. Lett. **112**, 112502 (2014).

[5] M. S. Basunia, Nucl. Data Sheets **127**, 69 (2015).

[6] M. Kimura, Phys. Rev. C **69**, 044319 (2004).

[7] M. Kimura, N. Furutachi, and Y. Kanada-En'yo, Nucl. Phys. A **834**, 482c (2010).

[8] M. Kimura, Phys. Rev. C **75**, 034312 (2007).

[9] N. Hinohara and J. Engel, Phys. Rev. C **90**, 031301(R) (2014).

[10] D. Gambacurta and D. Lacroix, Phys. Rev. C **91**, 014308 (2015).

[11] E. Ha and M.-K. Cheoun, Phys. Rev. C **94**, 054320 (2016).

[12] H. Morita and Y. Kanada-En'yo, Prog. Theor. Exp. Phys. **2016**, 103D02 (2016).

[13] A. B. Volkov, Nucl. Phys. **74**, 33 (1965).

[14] R. Tamagaki, Prog. Theor. Phys. **39**, 91 (1968).

[15] N. Yamaguchi, T. Kasahara, S. Nagata, and Y. Akaishi, Prog. Theor. Phys. **62**, 1018 (1979).

[16] H. Morita and Y. Kanada-En'yo, Phys. Rev. C **96**, 044318 (2017).

[17] J. D. MacArthur, A. J. Brown, P. A. Butler, L. L Green, C. J. Lister, A. N. James, P. J. Nolan, and J. F. Scharpey-Schafer, Can. J. Phys. **54**, 1134 (1976).